# Obtaining a Cartography of Impervious Surface Areas changes in the European Arctic using an EO-based cloud platform and machine learning: two case studies from Norway and Finland

George P, Petropoulos, Harokopio University of Athens, Department of Geography, Athens, Greece
Kleomenis, Kalogeropoulos, PhD, MSc, BSc, University of West Attica, Postdoctoral Research Fellow, Department of Surveying and Geoinformatics Engineering, Egaleo, Athens, Greece

## Obtaining a Cartography of Impervious Surface Areas Changes in the European Arctic using an EO-based cloud platform and machine learning: two case studies from Norway and Finland

*George P. Petropoulos[1], Katerina Dermosinoglou[1], Spyridon E. Detsikas[1], Kleomenis Kalogeropoulos[2],Giuseppe DiCaprio[3]*

*[1] Department of Geography, Harokopio University of Athens, El. Venizelou 70, Kallithea, 17671, Athens, Greece.*

*[2]Department of Surveying and Geoinformatics Engineering, University of West Attica, Egale, 12243 Athens, Greece*

*[3] PLANETGIS SKY S.R.L., Italy*

**Keywords:** *EO-PERSIST, ISA, Google Earth Engine, Remote Sensing, Arctic*

## INTRODUCTION

The term Impervious Surface Areas (ISA) is used to describe artificial surfaces that function as obstacles, hindering water intrusion into the soil. These features encompass numerous structures such as buildings, paved roads, driveways, sidewalks, parking lots, and rooftops (Petropoulos et al., 2015; Popa et al., 2022), serving as a crucial element in comprehending the environmental, ecological, and hydrological dimensions of urban planning. During the past 50 years, there has been a notable global proliferation of ISA, totaling approximately 0.62 million² kilometers from 1972 to 2019 (Huang et al., 2019). This surge aligns closely with the findings of the United Nations report (2018) on urbanization trends, revealing that in 2017, more than half, specifically 55% of the global population, resided in urban areas, with projections indicating a rise to 68% by 2050. Concurrently, it is also notable that human activities, such as energy exploitation and urban development, have notably contributed to the expansion of ISA in the Arctic region (Nguyen et al., 2021; Usman et al., 2022). Therefore, it is understood that these patterns underscore the significant correlation between ISA and human influence and thus it is of critical importance to systematically monitor ISA expansion.

that end, Earth Observation (EO) has been extensively utilized for ISA mapping, offering advantages in terms of time and cost efficiency. The Landsat archive has been pivotal in this regard, providing extensive and consistent medium-resolution EO data (Petropoulos et al., 2014; Chaudhuri et al., 2017; Schug et al., 2018; Cass et al., 2019; Cao et al., 2020; Xu et al., 2022). Besides Landsat, studies have employed Sentinel imagery (Feng & Fan, 2021), including both data from both optical and Synthetic Aperture Radar (SAR) data from the Sentinel missions (Shrestha et al., 2021; Wu et al., 2023). Various SAR datasets, such as ALOS/PALSAR (Attarchi, 2020), and TerraSAR-X (Zhang et al., 2016), have also been utilized, along with high-resolution images like IKONOS (Lu and Weng, 2009; Adetoro et al., 2022), WorldView (Adetoro et al., 2022), SPOT-5 (Xu, 2012), and GF-2 (Wang et al., 2022). Regarding hyperspectral sensors, their application in ISA extraction remains limited (Tang and Xu, 2017; Liu and Gu, 2017; Liu et al., 2020; Feng and Wang, 2018) but the use of the recently launched hyperspectral missions such as PRISMA and EnMAP looks promising. With new satellite missions, recording a wide range of the electromagnetic spectrum being constantly designed and launched, the volume of datasets that could be exploited for monitoring ISA has continuously been enriched. However, this creates new challenges in processing those EO datasets. To this end, cloud-based platforms such as Google Earth Engine, which enable the bulk processing of large volumes of geospatial datasets, could pose a significant solution. Yet, despite their potential, the use of cloud-based platforms is rather limited for ISA monitoring in the Arctic.

Along with the abundance of the EO satellites existing, there has been a wide variety of methods suitable for ISA mapping. Those techniques involve

index-based methods, pixel, and object-based methods (Feng et al., 2019; Pandey et al., 2019). The index-based methods consist of the most frequently used methods for ISA monitoring. EO-based indices exploit different spectral bands to distinguish and identify impervious surfaces, thus providing a variety of options for ISA mapping, especially using Landsat imagery. Among the indexes being more frequently used for such analysis are the Normalized Difference Built-up Index (NDBI) (Zha et al., 2003), the Index-based Built-up Index (IBI) (Xu, 2008) and the Normalized Difference Impervious Surface Index (NDISI) (Xu, 2010). In addition, the Combinational Built-up Index (CBI) and the Normalized Difference Impervious Surface Index (NDII), which were proposed by Sun et al. (2016) and Wang et al. (2015), respectively, are also used to map ISA. In addition, Fang et al. (2019) proposed the Ratio-based Impervious Surface Index (RISI), while Tian et al. (2018) introduced the Perpendicular Impervious Surface Index (PISI). Although their use is convenient and efficient, spectral indices face significant limitations in discriminating spectral similar objects, thus their use for ISA extraction is rather limited.

On the other hand, classification methods that separate pixels into impermeable and non-impermeable classes exploiting their spectral signatures, are widely used (Fang et al., 2019). Support vector machine (SVM) is one of the most used methods for ISA extraction and is known for its efficiency (Petropoulos et al., 2015; Feng et al., 2021). Also, studies have demonstrated the very good accuracy of SVM in the multitemporal mapping of ISAs, and many studies are confirming its effectiveness (Petropoulos et al., 2012; Petropoulos et al., 2012a; Petropoulos et al., 2012b; Mugiraneza et al, 2020; Fragou et al., 2020). In addition, the Random Forest (RF) method is considered satisfactory (Shrestha, 2021; Liu et al., 2020), while neural networks (NN) have been recognized as the most accurate for extracting structured ISAs using high-resolution satellite data ( Alem & Kumar, 2020). Deep learning methods have been effectively applied for ISA extraction, especially using high-resolution imagery such as WorldView and Pleiades (Huang et al., 2019). Several studies have also used deep learning for ISA mapping with moderate-resolution imagery such as Landsat (Parekh et al, 2021; Xu et al., 2022). In addition, Object-Based Image Analysis (OBIA) has been widely applied to ISA extraction, especially with high-resolution images (Petropoulos et al., 2012; Zhang et al., 2014). Although, there are several methods existing for ISA monitoring, the coupling of those techniques with the cloud-based platform is a promising field where its potential stays under investigation.

To this end, this study aims to investigate the potential of Google Earth Engine (GEE) coupled with a Support Vector Machine (SVM), to map ISA expansion in two Arctic cities over the time span of 30 years.

**Fig. 21.1** Selected study sites of (a) Tromso, Norway; (b) Rovaniemi, Finland

## STUDY AREA

In the present study, two Arctic settlements were selected as experimental sites, Tromso in Norway, and Rovaniemi in Finland (Figure 21.1). These two locations were chosen based on various criteria such as the population (the proposed threshold was >15.000) and the fact that Tromso is the second largest coastal city of northern Norway and Rovaniemi is the second largest city of northern Finland.

Tromso is an area in northern Norway that is a particularly important pole, as it is located north of the Arctic Circle and is the most densely populated city in northern Norway. With a thriving population of 77,544 (Statistics Norway, 2022), this affluent Arctic capital is connected to mainland Norway via the Tromso Bridge and Tromsø Tunnel and is also connected to the island of Kvalogia via the Sandnesund Bridge. The area is part of Troms County and has historical significance as a vital economic center, with origins dating back centuries. Before gaining city status in 1794, it served as the entry to the Arctic, for critical Arctic exploration. The Norwegian Sea, which surrounds the city, remains an important regional sea within the Arctic Ocean, providing rich resources and serving as a major transportation and communication route, contributing to a thriving local economy through its natural resources and profitable industries.

Rovaniemi is the administrative capital and commercial center of Finland's northernmost province, Lapland. It is located about 6 kilometers south of the Arctic Circle and is between the hills of Ounasvaara and Korkalovaara, at the confluence of the river Kemijoki and its tributary, the Ounasjoki. Due to its location near the Arctic Circle, Rovaniemi has a subarctic climate (Köppen Dfc) with short, pleasant summers, while winters are long, cold, and snowy. The city and the surrounding Rovaniemen maalaiskunta, which is the rural municipality of Rovaniemi, were incorporated into a single entity on 1 January 2006. The new municipality has an area of 8.017 km², thus making it the largest city in the European Union by land (). Rovaniemi has a population of

**Table 21.1** Acquired Landsat images description.

| Arctic Site | Date | Satellite | Cloud Cover (%) | Dataset |
|---|---|---|---|---|
| Tromso | | | 21 | LANDSAT/LT05/C02/T1_L2/ LT05_199011_19940731 |
| Tromso | | | 4.5 | LANDSAT/LC09/C02/T1_L2/ LC09_198011_20230630 |
| | | | 28 | LANDSAT/LT05/C02/T1_L2/ LT05_191013_19940707 |
| | | | 0.1 | LANDSAT/LC08/C02/T1_L2/ LC08_191013_20230808 |

approximately 65.000, while the sub-region has a population of approximately 69.000 inhabitants.

# DATASETS & PRE-PROCESSING
## DATASETS

In the present research, Landsat imagery was used for the multitemporal monitoring of ISA in the Arctic sites of Tromso, Norway, and Rovaniemi, Finland. Specifically, Landsat 5 Thematic Mapper (TM) and Landsat 8 Operated Land Imager (OLI), Collection 2 Surface Reflectance products were employed in this study. The selected images were acquired on anniversary dates during the summer months, as shown in Table x, to minimize the presence of significant cloud cover and ensure that the detected changes are not caused by natural or any other factors. The analysis was conducted covering a time span of 30 years, lasting from 1994 to 2023. Four images were chosen, two for each date, according to their cloud cover percentage with a 50% set (Table 21.1). Due to the geographic characteristics of the selected arctic areas, acquiring images with cloud cover below 10% posed a considerable challenge.

3.2 PRE-PROCESSING

All four Landsat images were obtained directly from the GEE platform. As the images were already atmospherically and geographically corrected, no additional processing was required. The first step was to create two boundary polygons in GEE, one for each settlement. The subsequent step involved the application of the Normalized Difference Water Index (NDWI), to mask out all water bodies while also the application of QA pixel masking to eliminate clouds, shadows, and unused pixels from all images. Also, a scale factor of 0.0000275 and an offset of -0.2 was applied, standardizing all values on a conceptual scale ranging from 0 to 1. In the final step of the pre-processing procedure, two mosaics were created, one for each date, on which would be applied the RF classification method. As the images for both study sites are derived from the same sensors, per date, the homogeneity of pixel values is ensured
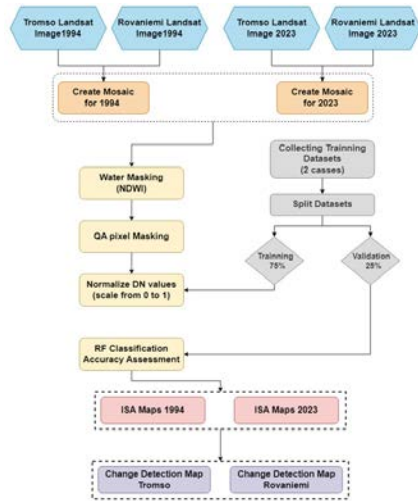
**Fig. 21.2** Methodology flowchart

and allows the generation of a common training–validation dataset and the development of the RF algorithm to both selected areas simultaneously.

## METHODS

## METHODOLOGY FRAMEWORK

The Random Forest (RF) method is used in this study, to classify ISA and detect changes from 1994 to 2023. The entire methodology process has been implemented through GEE cloud platform, as shown in Figure 21.2.

## RANDOM FOREST CLASSIFIER

Random Forest (RF) classifier is a machine learning algorithm that combines multiple trained decision trees to categorize unseen samples (Belgiu and Drăguț, 2016). Each tree gives an individual vote for the assignment, and the results are combined through a voting mechanism to determine the most popular class. Incorporating several classifiers into a classification set reduces variance and can provide more accurate results. Bagging ensembled methods, such as RF, aim to increase the stability and accuracy of integrated models while reducing variance. A new sample of predictors is obtained at each split, with a user-specified number of predictors. By expanding the random forest to a user-specified number of trees, RF generates trees with high variance and low bias. Each time an individual decision tree is generated, the best split in a random sample of predictions is selected. The final prediction will be the one that received the most votes. Increasing the number of trees improves the model performance, by minimizing overfitting and making predictions more accurate but also can scale up the training time and computational effort (Bera et al., 2023).

## CLASSIFICATION AND CHANGE DETECTION

Along the lines of other studies like Huang et al. (2021) and Li et al. (2021), it is also implemented herein binary classification which included the classes of Impervious and Non-Impervious, as the primary goal was to exclusively extract ISA. A pre-classification step was the generation of training–validation datasets. Two different datasets were created, each corresponding to one mosaic, by stratified sampling mainly based on the false–color composite (NIR, RED, GREEN bands) which better points out the ISA and SWIR bands. The dataset's points number follows the rule of 10N to 100N, where N is the number of bands used for the analysis. For Landsat 5 mosaic (6 bands), a range of 550 to 590 points were carefully selected, while for Landsat 8 mosaic (7 bands), almost 6500 points were selected, per class. Subsequently, the datasets were split into training and validation samples. 75% of the total points were allocated for training the classifier, with the remaining 25% used for validation. The RF machine learning classifier was trained and performed for all dates by default parameters, choosing 150 number of trees as the optimum number for the present analysis based on the data volume and the computational capacity.

The final phase of the entire process involved the development of post-classification Change Detection (CD) analysis in the GEE platform and the calculation of areas undergoing change. Post-classification comparison has been employed as the images were individually classified and the values of the pixels were converted in a conceptual scale. This approach reduces disparities between the dates, rendering it a robust method (Sun et al., 2008; Vivekananda et al., 2020). The ISA changes were mapped for each site separately and only alterations from Non-ISA to ISA were calculated. The changed areas were then quantified in $km^2$ according to the pixel size, and were turned into a percentage of change, relative to the size of the total study site. The results were visualized using ArcGIS Pro software and are presented in the next section.

## VALIDATION APPROACH

The evaluation of ISA was conducted through a comprehensive analysis of several statistical indices (Congalton, 1991), including Cohen's Kappa (Kc), Overall Accuracy (OA), Producer's Accuracy (PA), and User's Accuracy (UA). Kappa serves as a measure of agreement between the reference data and the classification, relative to the probability of agreement between the reference data and a random classifier. Overall accuracy quantifies the possibility of a pixel being accurately classified by the thematic map. The user's accuracy identifies pixels that, though not genuinely belonging to a reference class, are incorrectly assigned to other ground truth classes while the producer's accuracy carefully examines the pixels omitted from their reference class. Kappa (Kc) is a dimensionless metric ranging from 0 to 1, while the remaining statistical metrics are expressed as percentages (%). The values of OA, PA, and UA as well as the kappa coefficient were also automatically calculated in the GEE platform, by using the validation samples that were created. Those
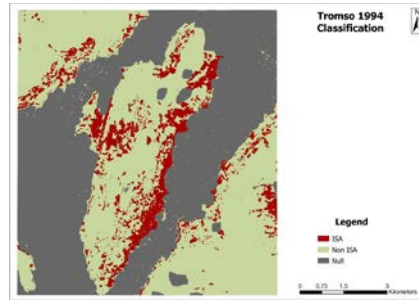
**Fig. 21.3** RF classification results for 1994, Tromso Norway (Pixels masked out are represented as "Null")

statistical metrics have also been used extensively in the literature in similar studies or classification accuracy assessments (e.g. Whyte et al., 2018; Lamine et al., 2018; Lekka et al, 2024).
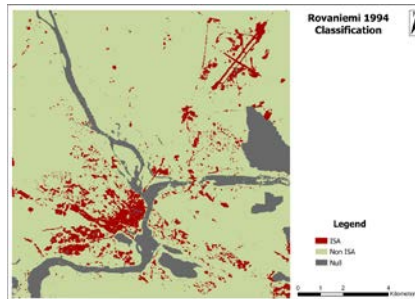
## RESULTS

The results of the RF classifier are presented in the next two figures (Figure 21.3 and Figure 21.4) for Tromso area and in Figure 21.5 and Figure 21.6 for Rovaniemi while the overall summary of the statistical results concerning the accuracy assessment of the classification is included in table Table 21.2. It should be mentioned that the term *Null* refers to pixels that have been excluded from the water and QA masking. The results of the classification in both experimental sites, reveal extensive urban growth from 1994 to 2023, registering an increase of approximately 24% in Tromso and 5,6% in Rovaniemi. It is also important to highlight the fact that in the case of Rovaniemi, the selected area is much more extensive than the one selected for Tromso, hence the ISA coverage rates are lower. More specifically, for Tromso, in 1994 (), the ISA area occupied 17,16% of the total area which is equal to almost 8 km². This ISA areas were mainly concentrated on the main territory of Tromso island, mapping the primary settlement of Tromso on the east and the airport area on the west, while sparsely composed ISA areas were detected in the eastern part of the study area, indicating the growth of the Tromsdalen settlement. In 2023 () the extent of ISA was estimated at almost 19,5 km², equivalent to 41% of the total area. A substantial expansion of ISA is observed in the main Tromso settlement which seems to occupy the whole Tromso island, while also the on eastern part of the study area is clearly mapped as the Tromsdalen settlement. A small number of bare soil pixels seems to be misclassified as ISA, in the north-western and south-eastern parts of the selected area.

In the case of Rovaniemi as well, a notable growth of ISA is observed. In 1994 (Figure 21.5) ISA covered almost 12,5 km², representing 10% of the total area. The city and the airport of Rovaniemi have been clearly detected, as well
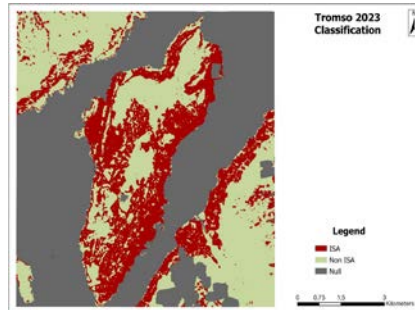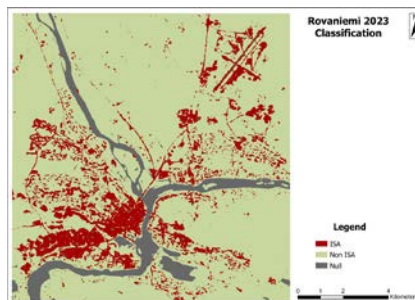
**Fig. 21.4**  RF classification results for 2023, Tromso Norway (Pixels masked out are represented as "Null")



**Fig. 21.5**  RF classification results for 1994, Rovaniemi Finland (Pixels masked out are represented as "Null")

as certain urban areas located near or along the riverside. In 2023 (Figure 6) the ISA percentage was equal to 15%, which corresponds to almost 12,5 km². The urban fabric of Rovaniemi appears more contiguous, with an observable increase of ISA mostly in the west part of the main settlement, but also in the northern part which links it with the airport. Fundamentally, a strong increase



**Fig. 21.6**  RF classification results for 2023, Rovaniemi Finland (Pixels masked out are represented as "Null")

**Table 21.2** Table 2. RF classifier accuracy assessment results (based on the confusion matrix)

|  | 1994 | | 2023 | |
| --- | --- | --- | --- | --- |
|  | UA (%) | PA (%) | UA (%) | PA (%) |
| ISA | 97,94 | 98,7 | 97,15 | 94,9 |
| Non ISA | 98,9 | 97,9 | 94,41 | 96,87 |
| OA (%) | 98,95 | | 95,83 | |
| kappa | 0,979 | | 0,916 | |
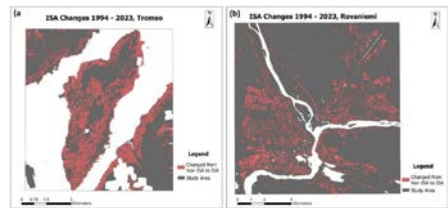


**Fig. 21.7** Change detection results for (a) Tromso, Norway; (b) Rovaniemi, Finland

of infrastructure such as the airport area and the road network are detected, but also an expansion of the urban fabric towards various directions.

The accuracy assessment for the classification was conducted using the confusion (error) matrix, which is presented in Table 21.2The following methodology in the present study leads to extremely accurate results, according to the following metrics. The OA reached 98,95% and 95,83% for 1994 and 2023 respectively, while kappa coefficient was 0,979 and 0,916. As for the rest of the accuracy metrics, PA took values from 96,87% to 98,7%, percentages that strongly indicate a high probability that the classification of each class aligns closely with reality. UA values ranged from 94,41% to 98,9% providing the accurate and subjective selection of training samples for both experimental sites.

Based on the classification results, a change detection analysis was performed to detect and map the ISA changes. During this methodological procedure were selected only changes from non-impervious to impervious classes, as that is the concern of the present study. In Figure 21.7 are presented the results of this analysis, based on RF classification.

As expected, because of the population growth in both experimental areas, ISA expansion is also recorded from 1994 to 2023. For Tromso, this growth is mainly detected across the island of Tromso where the primary settlement is located, but also on the eastern part of the city, as could be optically noticed in the classification results. Much the same applies to Rovaniemi, where a high rate of ISA expansion is observed, notably in areas around the riverbanks but also in the western part of the city and surrounding the airport area.

1. **DISCUSSION**

This study implemented an RF classifier with medium spatial resolution imagery from Landsat, specifically 5 and 8, to map ISA and detected changes from 1994 to 2023 in two Arctic experimental sites: Tromso, Norway, and Rovaniemi, Finland. This method, in contrast to the traditional classification and change detection methods, provides a semi-supervised tool for extracting ISA from Landsat data, detecting alterations in the imperviousness of the surface, and calculating the changed areas simply by selecting the appropriate images and providing the training samples. RF classifier is one of the most efficient and commonly used for land cover mapping, as shown by many studies (Shao et al., 2016; Shrestha et al., 2021; Shao et al., 2023).

According to the results, doth study sites have shown high levels of ISA expansion. The pattern of this expansion is apparently similar, as it is observed development occurring around the main settlements and also growth of infrastructure types, such as the road network, airports, etc. Depending on the city, demographic growth is also closely linked to the urban environments, but not necessarily to the continuous growth of built-up areas, as a part of the population tends to move to the urban fringe, causing the formation of metropolitan areas or larger urban areas (Mahtta et al., 2022). In terms of classifier efficiency, the highest overall accuracy achieved can be attributed to RF's ability to manage overfitting and noise effects, while also in the fact that a binary classification has been implemented. This is also confirmed in the present study, where the performance of the classifier is accurately high. RF yielded highly satisfactory results for the implemented study area, as indicated by the statistical metrics that were calculated. The findings presented in this study are like those observed in other research endeavors that used the RF technique with multispectral images in remote sensing applications (Xu et al., 2018; Guo et al., 2020; Dong et al., 2021).

In such a study, various factors may introduce errors that affect this current technique's performance. Clouds and cloud shadows have led to significant pixel removal in all images, potentially impacting the classification's quantitative results. Additionally, studies have highlighted a substantial confusion in spectral characteristics between impervious surfaces and bare soil, suggesting potential misclassification of pixels as ISA when they represent bare ground (Deng et al., 2020).

In the present study, the performance of the GEE platform is notable. Utilizing GEE, a semi-automated approach for processing and analyzing Landsat images was developed, integrating a machine learning RF algorithm for classification. Conducted entirely in a cloud environment, this ensured rapid execution, with only the final outcomes downloaded for visualization in ArcGIS Pro commercial software (ESRI, Redlands, USA). The distinctive features of GEE and similar cloud-based platforms offer promising prospects for ISA mapping on extensive geographical scales with promising potential exhibiting in monitoring the evolution of ISA and thus anthropogenic activity footprint in the whole Arctic region.

## 1. CONCLUSIONS

The Landsat images were suitable for this study due to their availability and pre-processing status. Regardless of their medium resolution, they yielded high accuracy rates, supporting the RF classifier's widespread use in land cover mapping, particularly for ISA. The classification outcomes were successful, boasting accuracy rates of 98.95% and 95.83% for each date. Additionally, the kappa coefficient values exceeded 0.9 for both dates, affirming the alignment between classification results and ground truth values. The classification results indicate a significant increase in ISA from 1994 to 2023, consistent with change detection analyses. Limitations include the lack of cloud-free images, leading to areas being obscured by clouds. Moreover, pixel value confusion between ISAs and bare soils presents challenges, as noted in the existing literature. Implementing the methodology in the GEE cloud platform is a major innovation. GEE efficiently manages large geospatial datasets and allows seamless integration and analysis of Landsat imagery across vast temporal and spatial scales. Utilizing GEE's cloud-based infrastructure reduces computational burdens, ensuring quicker analysis and results for ISA mapping from Landsat time series data. The combination of Landsat's multispectral data and the robust RF classifier within GEE improves ISA extraction accuracy and automation, facilitating change detection analyses. This comprehensive approach, leveraging GEE, Landsat data, and RF classifier, provides reliable and timely information essential for urban planning, environmental monitoring, and studying climate change impacts.

The study's findings significantly contribute to urban planning. The methodology used has the potential for real-time monitoring of ISA and can be adapted for various study areas with minimal parameter adjustments, making it a valuable tool for analyzing urban environments and aiding decision-making in fields like urban planning and natural hazards management.

### REFERENCES

Adetoro, O. I. O., Osarenren, V., & Popoola, S. O. (2022). Effects of Increasing Impervious Surface on Water Quality in Ile-Ife Urban Watershed, Southwestern Nigeria. Journal of Geoscience and Environment Protection, 10(12), 126–160. https://doi.org/10.4236/gep.2022.1012010

Alem, A., & Kumar, S. (2020). Deep Learning Methods for Land Cover and Land Use Classification in Remote Sensing: A Review. 2020 8th International Conference on Reliability, Infocom Technologies and Optimization (Trends and Future Directions) (ICRITO). https://doi.org/10.1109/icrito48877.2020.9197824

Attarchi, S. (2020). Extracting impervious surfaces from full polarimetric SAR images in different urban areas. International Journal of Remote Sensing, 41(12), 4644–4663. https://doi.org/10.1080/01431161.2020.1723178

Belgiu, M., & Drăguţ, L. (2016). Random forest in remote sensing: A review of applications and future directions. ISPRS Journal of Photogrammetry and Remote Sensing, 114, 24–31. https://doi.org/10.1016/j.isprsjprs.2016.01.011

Bera, D., Das Chatterjee, N., Bera, S., Ghosh, S., & Dinda, S. (2023). Comparative performance of Sentinel-2 MSI and Landsat-8 OLI data in canopy cover prediction using Random Forest model: Comparing model performance and tuning parameters. Advances in Space Research, 71(11), 4691–4709. https://doi.org/10.1016/j.asr.2023.01.027

Cao, X., Gao, X., Shen, Z., & Li, R. (2020). Expansion of Urban Impervious Surfaces in Xining City Based on GEE and Landsat Time Series Data. IEEE Access, 8, 147097–147111. https://doi.org/10.1109/access.2020.3013640

Cass, A., G.P. Petropoulos, K.P. Ferentinos, A. Pavlides & P.K. Srivastava (2019): Exploring the synergy between Landsat and ASAR towards improving thematic mapping accuracy of optical EO data. Applied Geomatics, 1-12, DOI: 10.1007/s12518-019-00258-7,

Congalton, R. G. (1991). A review of assessing the accuracy of classifications of remotely sensed data. Remote Sensing of Environment, 37(1), 35–46. https://doi.org/10.1016/0034-4257(91)90048-b

Deng, C., & Zhu, Z. (2020). Continuous subpixel monitoring of urban impervious surface using Landsat time series. Remote Sensing of Environment, 238, 110929. https://doi.org/10.1016/j.rse.2018.10.011

Dong, X., Meng, Z., Wang, Y., Zhang, Y., Sun, H., & Wang, Q. (2021). Monitoring Spatiotemporal Changes of Impervious Surfaces in Beijing City Using Random Forest Algorithm and Textural Features. Remote Sensing, 13(1), 153. https://doi.org/10.3390/rs13010153

Fang, H., Wei, Y., & Dai, Q. (2019). A Novel Remote Sensing Index for Extracting Impervious Surface Distribution from Landsat 8 OLI Imagery. Applied Sciences, 9(13), 2631. https://doi.org/10.3390/app9132631

Fang, H., Wei, Y., & Dai, Q. (2019). A Novel Remote Sensing Index for Extracting Impervious Surface Distribution from Landsat 8 OLI Imagery. Applied Sciences, 9(13), 2631. https://doi.org/10.3390/app9132631

Feng, B., & Wang, J. (2018). Evaluation of Unmixing Methods for Impervious Surface Area Extraction from Simulated EnMAP Imagery. IEEE Journal of Selected Topics in Applied Earth Observations and Remote Sensing, 11(6), 1777–1798. https://doi.org/10.1109/jstars.2018.2838449

Feng, G., Wang, K., Yin, D., Zou, S., & Wang, L. (2019). How to account for endmember variability in spectral mixture analysis of night-time light imagery? International Journal of Remote Sensing, 41(8), 3147–3161. https://doi.org/10.1080/01431161.2019.1699673

Feng, S., & Fan, F. (2021). Impervious surface extraction based on different methods from multiple spatial resolution images: a comprehensive compar-

ison. International Journal of Digital Earth, 14(9), 1148–1174. https://doi.org/10.1080/17538947.2021.1936227

Fragou, S., Kalogeropoulos, K., Stathopoulos, N., Louka, P., Srivastava, P. K., Karpouzas, S., P. Kalivas, D., & P. Petropoulos, G. (2020). Quantifying Land Cover Changes in a Mediterranean Environment Using Landsat TM and Support Vector Machines. Forests, 11(7), 750. https://doi.org/10.3390/f11070750

Guo, X., Zhang, C., Luo, W., Yang, J., & Yang, M. (2020). Urban Impervious Surface Extraction Based on Multi-Features and Random Forest. IEEE Access, 8, 226609–226623. https://doi.org/10.1109/access.2020.3046261

Huang, F., Yu, Y., & Feng, T. (2019). Automatic extraction of impervious surfaces from high resolution remote sensing images based on deep learning. Journal of Visual Communication and Image Representation, 58, 453–461. https://doi.org/10.1016/j.jvcir.2018.11.041

Huang, X., Li, J., Yang, J., Zhang, Z., Li, D., & Liu, X. (2021). 30 m global impervious surface area dynamics and urban expansion pattern observed by Landsat satellites: From 1972 to 2019. Science China Earth Sciences, 64(11), 1922–1933. https://doi.org/10.1007/s11430-020-9797-9

Lamine, S. G.P. Petropoulos, S.K. Singh, S. Szabo, N Bachari, P.K. Srivastava & S. Suman (2018): Quantifying Land Use/land Cover Spatio-temporal Landscape Pattern Dynamics from Hyperion Using SVMs Classifier and FRAGSTATS. Geocarto International, 33:8, 862-878, doi.org/10.1080/10106049.2017.1307460

Lekka, C., G.P. Petropoulos & S. E. Detsikas (2024): Appraisal of EnMAP hyperspectral imagery use in LULC mapping when combined with machine learning pixel-based classifiers. Environmental Modelling & Software, 173, 105956

Li, C., Shao, Z., Zhang, L., Huang, X., & Zhang, M. (2021). A Comparative Analysis of Index-Based Methods for Impervious Surface Mapping Using Multiseasonal Sentinel-2 Satellite Data. IEEE Journal of Selected Topics in Applied Earth Observations and Remote Sensing, 14, 3682–3694. https://doi.org/10.1109/jstars.2021.3067325

Liu, J., Liu, C., Feng, Q., & Ma, Y. (2020). Subpixel impervious surface estimation in the Nansi Lake Basin using random forest regression combined with GF-5 hyperspectral data. Journal of Applied Remote Sensing, 14(03). https://doi.org/10.1117/1.jrs.14.034515

Liu, S., & Gu, G. (2017). Improving the Impervious Surface Estimation from Hyperspectral Images Using a Spectral-Spatial Feature Sparse Representation and Post-Processing Approach. Remote Sensing, 9(5), 456. https://doi.org/10.3390/rs9050456

Liu, Z., Yang, J., & Huang, X. (2023). Landsat-derived impervious surface area expansion in the Arctic from 1985 to 2021. Science of the Total Environment, 905, 166966. https://doi.org/10.1016/j.scitotenv.2023.166966

Lu, D., & Weng, Q. (2009). Extraction of urban impervious surfaces from an IKONOS image. International Journal of Remote Sensing, 30(5), 1297–1311. https://doi.org/10.1080/01431160802508985

Mahtta, R., Fragkias, M., Güneralp, B., Mahendra, A., Reba, M., Wentz, E.A., & Seto, K.C. (2022). Urban land expansion: the role of population and economic growth for 300+ cities. npj Urban Sustain 2(5). https://doi.org/10.1038/s42949-022-00048-y

Mugiraneza, T., Nascetti, A., & Ban, Y. (2020). Continuous Monitoring of Urban Land Cover Change Trajectories with Landsat Time Series and LandTrendr-Google Earth Engine Cloud Computing. Remote Sensing, 12(18), 2883. https://doi.org/10.3390/rs12182883

Nguyen, T. L. H., Park, S. H., & Yeo, G. T. (2021). Keyword network analysis: Uncovering research trends on the Northern Sea Route. The Asian Journal of Shipping and Logistics, 37(3), 231–238. https://doi.org/10.1016/j.ajsl.2021.06.001

Pandey, P. C., Koutsias, N., Petropoulos, G. P., Srivastava, P. K., & Ben Dor, E. (2019). Land use/land cover in view of earth observation: data sources, input dimensions, and classifiers—a review of the state of the art. Geocarto International, 36(9), 957–988. https://doi.org/10.1080/10106049.2019.1629647

Parekh, J. R., Poortinga, A., Bhandari, B., Mayer, T., Saah, D., & Chishtie, F. (2021). Automatic Detection of Impervious Surfaces from Remotely Sensed Data Using Deep Learning. Remote Sensing, 13(16), 3166. https://doi.org/10.3390/rs13163166

Petropoulos, G. P., Arvanitis, K., & Sigrimis, N. (2012). Hyperion hyperspectral imagery analysis combined with machine learning classifiers for land use/cover mapping. Expert Systems with Applications, 39(3), 3800–3809. https://doi.org/10.1016/j.eswa.2011.09.083

Petropoulos, G. P., Kalaitzidis, C., & Prasad Vadrevu, K. (2012). Support vector machines and object-based classification for obtaining land-use/cover cartography from Hyperion hyperspectral imagery. Computers & Geosciences, 41, 99–107. https://doi.org/10.1016/j.cageo.2011.08.019

Petropoulos, G. P., Kontoes, C. C., & Keramitsoglou, I. (2012). Land cover mapping with emphasis to burnt area delineation using co-orbital ALI and Landsat TM imagery. International Journal of Applied Earth Observation and Geoinformation, 18, 344–355. https://doi.org/10.1016/j.jag.2012.02.004

Petropoulos, G.P., D.P. Kalivas, H. Georgopoulou, & P.K. Srivastava (2015): Urban Vegetation Cover Extraction from Hyperspectral Remote Sensing Imagery & GIS Spatial Analysis Techniques: the Case of Athens, Greece. Journal of Applied Remote Sensing, 9, 1-18, DOI 10.1117/1.JRS.9.096088

Petropoulos, G.P., H.M. Griffiths & D. Kalivas (2014): Quantifying Spatial and Temporal Vegetation Recovery Dynamics Following a Wildfire Event in a Mediterranean Landscape Using EO Data and GIS. Applied Geography, 50, 120-131, DOI 10.1016/j.apgeog.2014.02.006

Popa, A. M., Onose, D. A., Sandric, I. C., Dosiadis, E. A., Petropoulos, G. P., Gavrilidis, A. A., & Faka, A. (2022). Using GEOBIA and Vegetation Indices to Assess Small Urban Green Areas in Two Climatic Regions. Remote Sensing, 14(19), 4888. https://doi.org/10.3390/rs14194888

Sarkar Chaudhuri, A., Singh, P., & Rai, S. C. (2017). Assessment of impervious surface growth in urban environment through remote sensing estimates. Environmental Earth Sciences, 76(15). https://doi.org/10.1007/s12665-017-6877-1

Schug, F., Okujeni, A., Hauer, J., Hostert, P., Nielsen, J., & van der Linden, S. (2018). Mapping patterns of urban development in Ouagadougou, Burkina Faso, using machine learning regression modeling with bi-seasonal Landsat time series. Remote Sensing of Environment, 210, 217–228. https://doi.org/10.1016/j.rse.2018.03.022

Shao, Z., Cheng, T., Fu, H., Li, D., & Huang, X. (2023). Emerging Issues in Mapping Urban Impervious Surfaces Using High-Resolution Remote Sensing Images. Remote Sensing, 15(10), 2562. https://doi.org/10.3390/rs15102562

Shao, Z., Fu, H., Fu, P., & Yin, L. (2016). Mapping Urban Impervious Surface by Fusing Optical and SAR Data at the Decision Level. Remote Sensing, 8(11), 945. https://doi.org/10.3390/rs8110945

Shrestha, B., Stephen, H., & Ahmad, S. (2021). Impervious Surfaces Mapping at City Scale by Fusion of Radar and Optical Data through a Random Forest Classifier. Remote Sensing, 13(15), 3040. https://doi.org/10.3390/rs13153040

Sun, G., Chen, X., Jia, X., Yao, Y., & Wang, Z. (2016). Combinational Build-Up Index (CBI) for Effective Impervious Surface Mapping in Urban Areas. IEEE Journal of Selected Topics in Applied Earth Observations and Remote Sensing, 9(5), 2081–2092. https://doi.org/10.1109/jstars.2015.2478914

Sun, Z., Ma, R., & Wang, Y. (2008). Using Landsat data to determine land use changes in Datong basin, China. Environmental Geology, 57(8), 1825–1837. https://doi.org/10.1007/s00254-008-1470-2

Tang, F., & Xu, H. (2017). Impervious Surface Information Extraction Based on Hyperspectral Remote Sensing Imagery. Remote Sensing, 9(6), 550. https://doi.org/10.3390/rs9060550

Tian, Y., Chen, H., Song, Q., & Zheng, K. (2018). A Novel Index for Impervious Surface Area Mapping: Development and Validation. Remote Sensing, 10(10), 1521. https://doi.org/10.3390/rs10101521

Vivekananda, G., Swathi, R., & Sujith, A. (2020). Multi-temporal image analysis for LULC classification and change detection. European Journal of Remote Sensing, 54(sup2), 189–199. https://doi.org/10.1080/22797254.2020.1771215

Usman, M., Jahanger, A., Makhdum, M. S. A., Balsalobre-Lorente, D., & Bashir, A. (2022). How do financial development, energy consumption, natural resources, and globalization affect Arctic countries' economic growth and environmental quality? An advanced panel data simulation. Energy, 241, 122515. https://doi.org/10.1016/j.energy.2021.122515

Wang, M., Ding, W., Wang, F., Song, Y., Chen, X., & Liu, Z. (2022). A Novel Bayes Approach to Impervious Surface Extraction from High-Resolution Remote Sensing Images. Sensors, 22(10), 3924. https://doi.org/10.3390/s22103924

Wang, Z., Gang, C., Li, X., Chen, Y., & Li, J. (2015). Application of a normalized difference impervious index (NDII) to extract urban impervious surface fea-

tures based on Landsat TM images. International Journal of Remote Sensing, 36(4), 1055–1069. https://doi.org/10.1080/01431161.2015.1007250

Whyte, A., K. Feredinos & G.P. Petropoulos (2018): A New Synergistic Approach for Monitoring Wetlands Using Sentinels -1 and 2 data With Object-based Machine Learning Algorithms. Environmental Modelling & Software, 104, 40-57, doi.org/10.1016/j.envsoft.2018.01.023

Wu, W., Guo, S., Shao, Z., & Li, D. (2023). Urban Impervious Surface Extraction Based on Deep Convolutional Networks Using Intensity, Polarimetric Scattering and Interferometric Coherence Information from Sentinel-1 SAR Images. Remote Sensing, 15(5), 1431. https://doi.org/10.3390/rs15051431

Xu, H. (2008). A new index for delineating built  up land features in satellite imagery. International Journal of Remote Sensing, 29(14), 4269–4276. https://doi.org/10.1080/01431160802039957

Xu, H. (2010). Analysis of Impervious Surface and its Impact on Urban Heat Environment using the Normalized Difference Impervious Surface Index (NDISI). Photogrammetric Engineering & Remote Sensing, 76(5), 557–565. https://doi.org/10.14358/pers.76.5.557

Xu, H. (2012). Rule-based impervious surface mapping using high spatial resolution imagery. International Journal of Remote Sensing, 34(1), 27–44. https://doi.org/10.1080/01431161.2012.703343

Xu, H., Xiao, X., Qin, Y., Qiao, Z., Long, S., Tang, X., & Liu, L. (2022). Annual Maps of Built-Up Land in Guangdong from 1991 to 2020 Based on Landsat Images, Phenology, Deep Learning Algorithms, and Google Earth Engine. Remote Sensing, 14(15), 3562. https://doi.org/10.3390/rs14153562

Xu, Z., Chen, J., Xia, J., Du, P., Zheng, H., & Gan, L. (2018). Multisource Earth Observation Data for Land-Cover Classification Using Random Forest. IEEE Geoscience and Remote Sensing Letters, 15(5), 789–793. https://doi.org/10.1109/lgrs.2018.2806223

Zha, Y., Gao, J., & Ni, S. (2003). Use of normalized difference built-up index in automatically mapping urban areas from TM imagery. International Journal of Remote Sensing, 24(3), 583–594. https://doi.org/10.1080/01431160304987

Zhang, H., Lin, H., Li, Y., Zhang, Y., & Fang, C. (2016). Mapping urban impervious surface with dual-polarimetric SAR data: An improved method. Landscape and Urban Planning, 151, 55–63. https://doi.org/10.1016/j.landurbplan.2016.03.009

Zhang, Y., Zhang, H., & Lin, H. (2014). Improving the impervious surface estimation with combined use of optical and SAR remote sensing images. Remote Sensing of Environment, 141, 155–167. https://doi.org/10.1016/j.rse.2013.10.028

# Data-Driven Earth Observation for Disaster Management
## From Theory to Practical Applications
**Edited by Xiao Huang, Siqin Wang, Kleomenis Kalogeropoulos, and Andreas Tsatsaris**
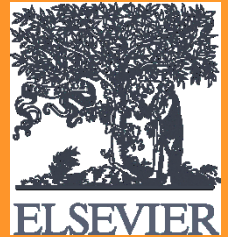
ELSEVIER

To whom it may concern

January 25th, 2024

# Acceptance letter

I am pleased to inform you that your chapter has been accepted for publication by Elsevier, and will be included in the book "**Data-Driven Earth Observation for Disaster Management: From Theory to Practical Applications**", edited by Xiao Huang, Siqin Wang, Kleomenis Kalogeropoulos, and Andreas Tsatsaris.

Your submission entitled "**Obtaining a Cartography of Impervious Surface Areas Changes in the European Arctic using an EO-based cloud platform and machine learning: two case studies from Norway and Finland**" by George P. Petropoulos, Katerina Dermosinoglou, Spyridon E. Detsikas, Kleomenis Kalogeropoulos, Giuseppe DiCaprio is extremely relevant and of high quality, matching Elsevier's standards exactly.

Production will begin soon on **Data-Driven Earth Observation for Disaster Management: From Theory to Practical Applications (ISBN: 9780443338038)**, and we expect the book to be published in 2026.

Thank you for your excellent submission, we are delighted to include it in the book.

Thank you for your continued patience throughout the production process.

On behalf of the Editors,

Prof. Dr. Andreas Tsatsaris

ELSEVIER